J. Fluid Mech. (2006), *vol.* 561, *pp.* 391–416. © 2006 Cambridge University Press
doi:10.1017/S0022112006000760 Printed in the United Kingdom

Subharmonic resonance of a trapped wave near a vertical cylinder in a channel

By YILE LI[1] AND CHIANG C. MEI[2]

[1]Department of Mechanical Engineering, Massachusetts Institute of Technology, Cambridge, MA 02139, USA

[2]Department of Civil and Environmental Engineering, Massachusetts Institute of Technology, Cambridge, MA 02139, USA

(Received 10 September 2005 and in revised form 23 January 2006)

It is known that perfectly trapped surface waves exist at certain eigenfrequencies near a vertical cylinder in a long channel, or an infinite and periodic array of vertical cylinders, and excitation by incident waves of the same frequency is not possible according to the linear theory. We present a nonlinear theory whereby a trapped wave near a cylinder in a channel is excited subharmonically by an incident wave of twice the eigenfrequency. The effects of geometrical parameters on the initial growth of resonance and the final amplification are studied in detail.

1. Introduction

The linearized theory of water-wave trapping either by a stationary body in a channel or by an infinite and periodic array of fixed bodies has been extensively treated by Evans and his associates in the past decade. Specifically, Evans & Linton (1991) derived the eigenwavenumber k' and potentials of trapped modes around a vertical cylinder of rectangular cross-section standing at the centre of a channel of width $2d'$. Within the range $0 < k'd' < \pi/2$ below the cutoff of propagating waves, there can be a symmetric mode as well as an antisymmetric mode with respect to the vertical centre-plane perpendicular to the channel walls. Subsequently, Callan, Linton & Evans (1991) also found a symmetric trapped mode around a circular cylinder of radius a' in a channel in the same range of $k'd'$. The predicted eigenfrequency has been verified in a wave-tank experiment by an impulsive displacement of the cylinder (Retzler 2001). Another antisymmetric mode was later found to exist in $0.81 < a'/d' < 1$ by Evans & Porter (1999). Maniar & Newman (1997) also found above the cutoff with $k'd' \sim \pi$, a *Dirichlet mode* which satisfies the condition of zero-potential on the channel walls. This mode is relevant to sound waves in a channel and to water waves around an infinite array of cylinders spaced at $2d'$ apart. Mathematical aspects and other extensions have been reported by Linton & Evans (1992*a*), Evans, Levitin & Vassiliev (1994), Evans & Porter (1997, 1998) and by Utsunomiya & Eatock Taylor (1999). The occurrence of these modes around a multi-legged structure such as an offshore airport may pose a threat to the safety of the installation, hence it is of engineering interest. According to the linearized theory, perfectly trapped modes cannot be resonated by incident waves of the same frequency, since no propagation is possible below cutoff. However, in the case of a finite number of periodically spaced cylinders in an infinite sea, there is no cutoff and trapping is imperfect. Synchronous resonance can be predicted by a linear theory as in Maniar & Newman

(1997). However, amplification at resonance is found to increase with the number of cylinders, when real fluid effects are not included. In a laboratory experiment by Kagemoto *et al.* (2002), viscous dissipation was shown to reduce or to obliterate the high peaks predicted by the linearized potential theory. Away from the trapping frequency, scattering of monochromatic waves by one or more cylinders in a channel, or by an infinite array in unbounded sea, is a problem of diffraction grating, and has been treated by Linton & Evans (1990, 1992*b*, 1993) and McIver & Bennett (1993).

In coastal oceanography it is known that trapped edge waves can also be present on a sloping beach. In the ideal case of an infinite and uniform beach, trapping is also perfect. It was found from laboratory experiments by Galvin (1965) that an edge wave can be resonated subharmonically by incident waves of twice the frequency. Theoretical explanations were given later by Guza & Davis (1974), Guza & Bowen (1976), Minzoni & Whitham (1977) and Rockliff (1978). Of recent interest in coastal engineering is the case of mobile barriers for protecting the venice lagoon from storm tides. Each of the four planned barriers is a series of twenty closely aligned hollow gates across an inlet. For reducing wave forces on the supporting structures, all gates are allowed to swing about a common axis on the seabed, but are otherwise unattached to one another. Experiments have revealed, however, that normally incident sea waves can force the neighbouring gates to oscillate in opposite phases, at half the frequency. This oscillation, of course, affects the intended purpose of the gate system as a dam. The cause for this oscillation was later found to be the existence of trapped modes owing to the periodic and mobile construction (Mei *et al.* 1994). A nonlinear theory for monochromatic incident waves, similar to the subharmonic resonance of edge waves, has been given by Sammarco, Tran & Mei (1997*a*), and confirmed by laboratory experiments. Extension to narrow-banded incident waves further revealed that resonance can become chaotic, which has also been verified by experiments (Sammarco *et al.* 1997 *b*).

In view of the possible importance to offshore structures involving a periodic array of cylinders, we present here a nonlinear theory for subharmonic resonance of waves trapped by a vertical cylinder in a channel, which is mathematically equivalent to an infinite array of periodically spaced cylinders. The evolution equation for the amplitude of the trapped mode is found analytically to be of the Landau–Stuart form. The main task of calculating the coupling coefficients is achieved by solving a number of scattering or radiation problems. By numerical solution of these problems, the effects of the geometry on the resonance characteristics are examined.

2. Boundary-value problem

Let physical quantities be identified by primes. We consider a bottom-mounted circular cylinder of radius a' fixed at the centre of a channel of width $2d'$ and depth h'. Let a Cartesian coordinate system be chosen such that the (x', y')-plane coincides with the still free surface and z' points upward along the cylinder axis, as shown in figure 1. A train of plane waves of amplitude A' arrives along the positive x'-axis towards the cylinder.

Let the fluid be incompressible and inviscid, and the flow be irrotational. Normalized variables defined below without primes will be employed throughout,

$$\left.\begin{aligned} t = \sqrt{\frac{g}{d'}}t', \qquad & (x, y, z) = \frac{(x', y', z')}{d'}, \quad (h, a) = \frac{(h', a')}{d'}, \\ \zeta = \zeta'/\sqrt{A'd'} \qquad & \Phi = \frac{1}{d'\sqrt{gA'}}\Phi', \end{aligned}\right\} \tag{2.1}$$

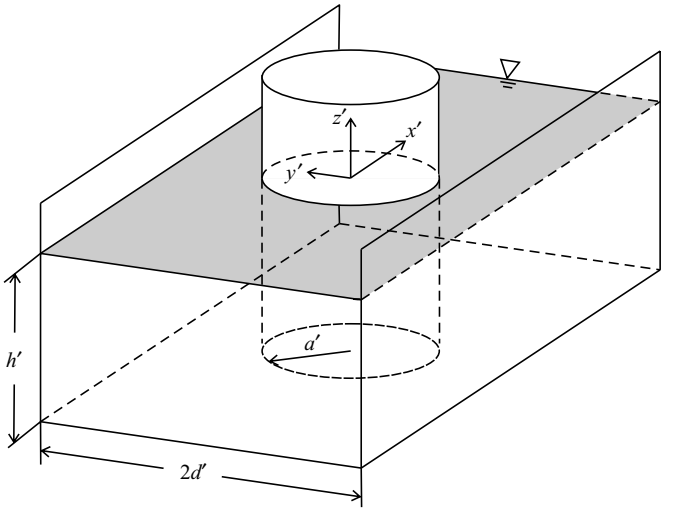

FIGURE 1. Circular cylinder at the centre of an open channel.

where ζ' and Φ' represent the free-surface height and velocity potential-respectively. In dimensionless variables, the boundary-value problem is governed by

$$\nabla^2\Phi = 0, \tag{2.2}$$

in the fluid and

$$\frac{\partial\Phi}{\partial z} + \frac{\partial^2\Phi}{\partial t^2} + 2\epsilon\,\nabla\Phi\cdot\nabla\frac{\partial\Phi}{\partial t} + \epsilon^2\,\nabla\Phi\cdot\nabla\left(\frac{\nabla\Phi\cdot\nabla\Phi}{2}\right) = 0, \quad z = \epsilon\zeta, \tag{2.3}$$

on the free surface, where ϵ denotes the small ratio of wave amplitude to channel half-width

$$\epsilon = \sqrt{\frac{A'}{d'}} \ll 1. \tag{2.4}$$

We also require no flux

$$\frac{\partial\Phi}{\partial r} = 0, \quad r = a, \tag{2.5}$$

on the cylinder,

$$\frac{\partial\Phi}{\partial y} = 0, \quad y = \pm 1, \tag{2.6}$$

on the sidewalls, and

$$\frac{\partial\Phi}{\partial z} = 0, \quad z = -h, \tag{2.7}$$

on the seabed. From the Bernoulli equation, the free-surface elevation is

$$\zeta = -\frac{\partial\Phi}{\partial t} - \frac{\epsilon}{2}\nabla\Phi\cdot\nabla\Phi \quad \text{on} \quad z = \epsilon\zeta. \tag{2.8}$$

Under the assumption of small-amplitude waves, Taylor expansion of the combined free-surface condition (2.3) about the undisturbed water level $z=0$ gives:

$$\begin{aligned}\frac{\partial \Phi}{\partial z}+\frac{\partial^2\Phi}{\partial t^2}+\epsilon\frac{\partial}{\partial t}(\nabla\Phi\cdot\nabla\Phi)-\epsilon\frac{\partial\Phi}{\partial t}\frac{\partial}{\partial z}\left(\frac{\partial\Phi}{\partial z}+\frac{\partial^2\Phi}{\partial t^2}\right)\\ +\epsilon^2\left(-\tfrac{1}{2}\nabla\Phi\cdot\nabla\Phi+\frac{\partial\Phi}{\partial t}\frac{\partial^2\Phi}{\partial t\partial z}\right)\frac{\partial}{\partial z}\left(\frac{\partial\Phi}{\partial z}+\frac{\partial^2\Phi}{\partial t^2}\right)\\ -\epsilon^2\frac{\partial\Phi}{\partial t}\frac{\partial^2}{\partial t\partial z}(\nabla\Phi\cdot\nabla\Phi)+\tfrac{1}{2}\epsilon^2\left(\frac{\partial\Phi}{\partial t}\right)^2\frac{\partial^2}{\partial z^2}\left(\frac{\partial\Phi}{\partial z}+\frac{\partial^2\Phi}{\partial t^2}\right)\\ +\tfrac{1}{2}\epsilon^2\nabla\Phi\cdot\nabla(\nabla\Phi\cdot\nabla\Phi)=O(\epsilon^3),\quad z=0\end{aligned}\tag{2.9}$$

while (2.8) becomes

$$\begin{aligned}\zeta=&-\frac{\partial\Phi}{\partial t}-\epsilon\left\{\tfrac{1}{2}\nabla\Phi\cdot\nabla\Phi-\frac{\partial\Phi}{\partial t}\frac{\partial^2\Phi}{\partial t\partial z}\right\}\\ &+\frac{\epsilon^2}{2}\frac{\partial}{\partial z}\left\{\Phi_t\left(\nabla\Phi\cdot\nabla\Phi-\Phi_t\frac{\partial\Phi_t}{\partial z}\right)\right\}+O(\epsilon^3),\quad z=0.\end{aligned}\tag{2.10}$$

3. Perturbation problems

Similar to the excitation of trapped waves along a sloping beach (Minzoni & Whitham 1977) or around the mobile gates of Venice (Sammarco *et al.* 1997*a*, *b*), it can be shown that a trapped wave of natural frequency ω and amplitude $O(1)$ can be excited nonlinearly by an incident and scattered wave system of order ϵ at frequency 2ω. The long time scale of resonant growth is of the order $1/\omega\epsilon^2$.

Upon introducing the slow time $\tau=\epsilon^2 t$ and the multiple-scale expansions

$$\Phi=\Phi_1(x,y,z;t,\tau)+\epsilon\Phi_2(x,y,z;t,\tau)+\epsilon^2\Phi_3(x,y,z;t,\tau)+O(\epsilon^3),\tag{3.1}$$

$$\zeta=\zeta_1(x,y;t,\tau)+\epsilon\zeta_2(x,y;t,\tau)+\epsilon^2\zeta_3(x,y;t,\tau)+O(\epsilon^3),\tag{3.2}$$

we obtain from (2.2)–(2.7) and the free-surface condition (2.9), the governing perturbation equations for the first three orders, $i=1,2,3$:

$$\nabla^2\Phi_i=0\qquad\text{in the fluid,}\tag{3.3}$$

$$\frac{\partial\Phi_i}{\partial z}+\frac{\partial^2\Phi_i}{\partial t^2}=\mathscr{F}_i\quad\text{on}\quad z=0,\tag{3.4}$$

$$\frac{\partial\Phi_i}{\partial n}=0\qquad\text{on } r=a;\ y=\pm1;\text{ and } z=-h.\tag{3.5}$$

The forcing functions $\mathscr{F}_i$ on the free surface are:

$$\mathscr{F}_1=0,\tag{3.6}$$

$$\mathscr{F}_2=\frac{\partial\Phi_1}{\partial t}\frac{\partial}{\partial z}\left(\frac{\partial\Phi_1}{\partial z}+\frac{\partial^2\Phi_1}{\partial t^2}\right)-\frac{\partial}{\partial t}(\nabla\Phi_1\cdot\nabla\Phi_1);\tag{3.7}$$

$$\mathscr{F}_3 = -2\frac{\partial^2\Phi_1}{\partial t\partial\tau} + \frac{\partial\Phi_1}{\partial t}\frac{\partial}{\partial z}\left(\frac{\partial\Phi_2}{\partial z} + \frac{\partial^2\Phi_2}{\partial t^2}\right) + \frac{\partial\Phi_2}{\partial t}\frac{\partial}{\partial z}\left(\frac{\partial\Phi_1}{\partial z} + \frac{\partial^2\Phi_1}{\partial t^2}\right)$$
$$-2\frac{\partial}{\partial t}(\nabla\Phi_1\cdot\nabla\Phi_2) + \tfrac{1}{2}\nabla\Phi_1\cdot\nabla\Phi_1\frac{\partial}{\partial z}\left(\frac{\partial\Phi_1}{\partial z} + \frac{\partial^2\Phi_1}{\partial t^2}\right)$$
$$-\frac{\partial\Phi_1}{\partial t}\frac{\partial^2\Phi_1}{\partial t\partial z}\frac{\partial}{\partial z}\left(\frac{\partial\Phi_1}{\partial z} + \frac{\partial^2\Phi_1}{\partial t^2}\right) - \tfrac{1}{2}\left(\frac{\partial\Phi_1}{\partial t}\right)^2\frac{\partial^2}{\partial z^2}\left(\frac{\partial\Phi_1}{\partial z} + \frac{\partial^2\Phi_1}{\partial t^2}\right)$$
$$+\frac{\partial\Phi_1}{\partial t}\frac{\partial^2}{\partial t\partial z}(\nabla\Phi_1\cdot\nabla\Phi_1) - \tfrac{1}{2}\nabla\Phi_1\cdot\nabla(\nabla\Phi_1\cdot\nabla\Phi_1). \tag{3.8}$$

The first- and second-order free-surface elevation are obtained from (2.10):

$$\zeta_1 = -\frac{\partial\Phi_1}{\partial t}, \tag{3.9}$$

$$\zeta_2 = -\frac{\partial\Phi_2}{\partial t} - \tfrac{1}{2}\nabla\Phi_1\cdot\nabla\Phi_1 + \frac{\partial\Phi_1}{\partial t}\frac{\partial^2\Phi_1}{\partial t\partial z}. \tag{3.10}$$

4. The trapped mode at the first order

At the first order, the boundary-value problem is homogeneous. Let the eigenfunction be expressed as

$$\Phi_1 = \frac{B}{2}\varphi_1(x, y, z)\mathrm{e}^{-\mathrm{i}\omega t} + * = \frac{B}{2\,\mathrm{i}\omega}\frac{\cosh k(z+h)}{\cosh kh}\eta(x, y)\mathrm{e}^{-\mathrm{i}\omega t} + *, \tag{4.1}$$

where $B(\tau)$ is the complex amplitude. Hereinafter, asterisks denote complex conjugates. The spatial factors φ_1 and η satisfy the no-flux condition on channel walls and are antisymmetric about the channel middle plane $y = 0$. As shown in Callan *et al.* (1991), a trapped mode symmetric in x exists for all cylinder radius $0 < a < 1$ below the cutoff wavenumber $k < \pi/2$. Only in the small range of $0.81 < a < 1$, a second trapped mode antisymmetric in x with a different eigenfrequency exists (Evans & Porter 1999). In the present study, we focus our attention only on the x-symmetric mode; the second mode can be treated similarly. Without loss of generality, we assume φ_1 to be real and η purely imaginary.

The wavenumber k is related to ω by the dispersion relation:

$$\omega^2 = k\tanh kh. \tag{4.2}$$

For a vertical cylinder of circular cross-section, the eigenwavenumber k depends only on the dimensionless radius a. Through the dispersion relation (4.2), the eigenfrequency ω depends on the water depth in addition. From figure 2 of Callan *et al.* (1991), the following features for the eign-wavenumber k are known.

When $a \to 0$, k approaches the cutoff value $\pi/2$. At this limit, the free-surface amplitude becomes uniform in x, hence the wave is no longer trapped. As the cylinder radius a increases from 0, k decreases slowly from $\pi/2$ to the minimum $k \approx 1.32$ at $a = 0.76$. Beyond that radius, k increases monotonically to $k \approx 1.43$ at $a = 1$, when the cylinder blocks the channel. For convenience of physical discussion, we show in figure 2 the trapped-mode frequency as a function of a for different water depth h as calculated from (4.2). For the same cylinder radius, ω first increases with depth linearly as ($\omega \approx \sqrt{h}k$), and then approaches its limit $\sqrt{k}$ as the water becomes very deep ($\omega \approx \sqrt{k}$).

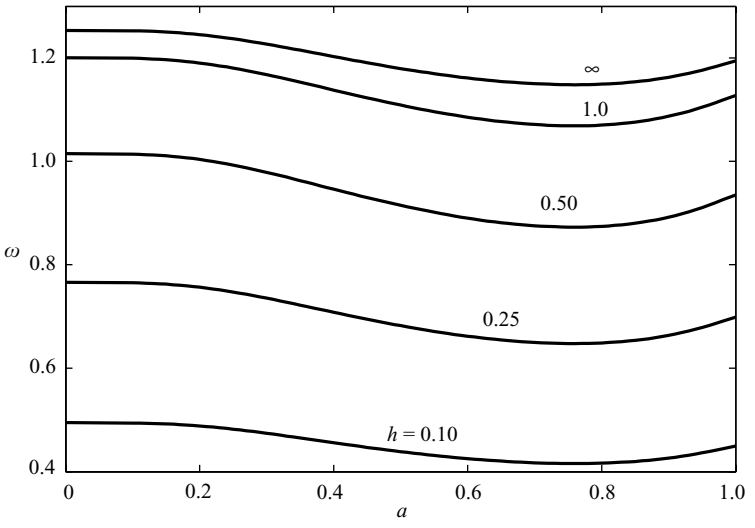

FIGURE 2. Dependence of the trapped mode wave frequency ω on the radius of circular cylinder a and the water depth h.

We remark that, for any body geometry, the eigenvalue problem can be solved numerically by the hybrid-element technique described for a more complex problem in Appendix A. Let the channel be divided into the near field around the cylinder, and the far field $|x| > L$ away from the cylinder. The basic idea is to employ two-dimensional finite elements only near the body where the geometry is complex, and analytical representations via eigenfunction expansions in the far field. For later use we record the far-field surface displacement,

$$\eta^{\pm} = \sum_{m=1}^{\infty} D_m \exp\left(\kappa_m(\mp x + L)\right) \sin\left(m - \tfrac{1}{2}\right) \pi y, \quad x \gtrless \pm L, \tag{4.3}$$

where

$$\kappa_m = \sqrt{\left(m - \tfrac{1}{2}\right)^2 \pi^2 - k^2}, \quad m = 1, 2, \ldots \tag{4.4}$$

is real. The expansion coefficients D_m in the far fields are found by a variational method along with the nodal unknowns in the near field.

5. Diffraction and radiation at the second order

At second order, the free-surface condition is no longer homogeneous:

$$\frac{\partial \Phi_2}{\partial z} + \frac{\partial^2 \Phi_2}{\partial t^2} = \mathscr{F}_2 \quad \text{on } z = 0, \tag{5.1}$$

where $\mathscr{F}_2$ is given in (3.7). Substituting (4.1) into (3.7), we obtain

$$\mathscr{F}_2 = \frac{B^2}{2} q \mathrm{e}^{-2\mathrm{i}\omega t} + *, \tag{5.2}$$

with

$$q = \frac{1}{2\mathrm{i}\omega}\left(2\eta_x^2 + 2\eta_y^2 + (3\omega^4 - k^2)\eta^2\right). \tag{5.3}$$

We remark that, for the trapped mode, η is even in x but odd in y, hence q is even in both x and y.

Let the total solution be the sum of three parts

$$\Phi_2 = \Phi_I + \Phi_S + \Phi_Q. \tag{5.4}$$

where Φ_I and Φ_S are the incident and scattered wave potentials, respectively, and Φ_Q is the radiated wave forced on the free surface by quadratic interactions. These parts are treated separately below.

5.1. *The diffraction problem Φ_I and Φ_S*

The diffraction problem is standard in the linearized theory. Let the incident and scattered wave potentials be expressed by

$$\begin{pmatrix} \Phi_I \\ \Phi_S \end{pmatrix} = \frac{A}{4\mathrm{i}\omega} \frac{\cosh K(z+h)}{\cosh Kh} \begin{pmatrix} \eta_I(x) \\ \eta_S(x, y) \end{pmatrix} \mathrm{e}^{-2\mathrm{i}\omega t} + *, \tag{5.5}$$

where the incident wave elevation is

$$\eta_I = \mathrm{e}^{\mathrm{i}Kx}, \tag{5.6}$$

and K satisfies the dispersion relation with 2ω:

$$K \tanh Kh = 4\omega^2. \tag{5.7}$$

A small detuning is allowed so that

$$A = \mathrm{e}^{-2\mathrm{i}\epsilon^2\Omega t} = \mathrm{e}^{-2\mathrm{i}\Omega\tau}, \tag{5.8}$$

with $2\epsilon^2\Omega$ representing the detuning frequency.

The spatial factor η_S for the scattered wave is governed by the two-dimensional equations,

$$\left(\frac{\partial^2}{\partial x^2} + \frac{\partial^2}{\partial y^2} + K^2\right)\eta_S = 0, \qquad (x, y) \in S_F, \tag{5.9}$$

$$\frac{\partial \eta_S}{\partial n} = -\frac{\partial \mathrm{e}^{\mathrm{i}Kx}}{\partial n} \qquad \text{on } r = a, \tag{5.10}$$

$$\frac{\partial \eta_S}{\partial y} = 0 \qquad \text{on } y = \pm 1, \tag{5.11}$$

and the radiation condition at two infinities. This problem is solved numerically by the hybrid-element method (see Appendix A). In the near field, defined by two vertical cross-sectional planes $x = \pm L$ enclosing the cylinder, two-dimensional finite elements are used. Outside these planes, the following eigenfunction expansions are used for the scattered wave

$$\eta_S^{\pm} = \sum_{m=0}^{\infty} S_m^{\pm} \mathrm{e}^{\pm \mathrm{i}\beta_m x} \cos m\pi y, \qquad x \gtrless \pm L, \tag{5.12}$$

where $S_m^{\pm}$ are unknown coefficients and

$$\beta_m = \sqrt{K^2 - m^2\pi^2}, \qquad m = 0, 1, 2, \ldots. \tag{5.13}$$

Let $\overline{m}$ be the largest integer for which $K > m\pi$, then for $m = 0, 1, \ldots, \overline{m}$, β_m are real. The corresponding terms in the series represent outgoing waves. For $m = \overline{m}+1, \ldots, \infty$, $\beta_m = \mathrm{i}\sqrt{m^2\pi^2 - K^2}$ are imaginary, the corresponding terms represent evanescent modes. We note that at the special values $K = m\pi$, the mth scattered modes are at

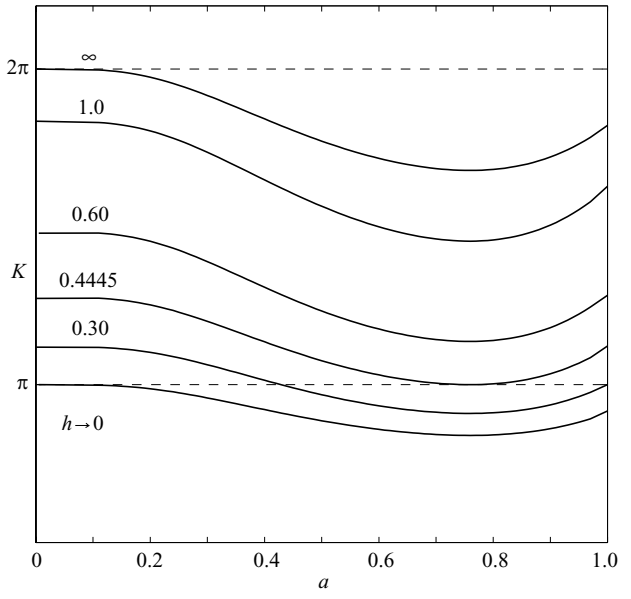

FIGURE 3. Dependence of K on the cylinder radius a and the water depth h.

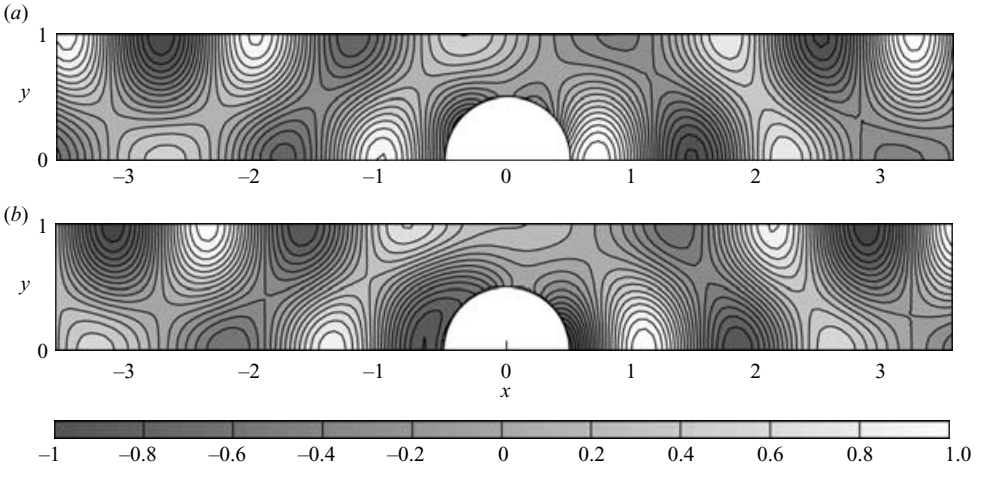

FIGURE 4. Scattered-wave free-surface elevation η_S, $a = 0.5$, $2\omega = 2.218$. (a) Real part; (b) imaginary part. η_S is symmetric about $y = 0$.

the cutoff threshold. Recall that the eigenfrequency ω is a function of a and h. Hence the dependence of K on a and h is found from (5.7). We plot K *vs.* a for a wide range of h in figure 3. When water is shallow, $h \leqslant 0.30$, the (K, a) curve crosses the first cutoff wavenumber $K = \pi$ once at a small a. If $0.30 < h < 0.4445$, there exist two radii at which the incident wavenumber gives rise to cutoff at $K = \pi$. As the depth increases, $\pi < K < 2\pi$ and no cutoff wavenumber will be encountered.

The hybrid-element numerical scheme is used to compute the scattered waves near and away from the cylinder for a wide range of frequencies. Sample numerical results for the scattered wave are presented in figure 4 for $a = 1/2$ and $h = 1$. From figure 2, the trapped wave frequency is found to be $\omega = 1.109$ so that the incident wave has the frequency $2\omega = 2.218$.

5.2. *Radiation due to quadratic forcing : Φ_Q*

Since the forcing function on the free surface (5.2) contains only the second harmonic,

$$\Phi_Q = \tfrac{1}{2}B^2\varphi_Q e^{-2i\omega t} + *. \tag{5.14}$$

From (3.3)–(3.5), φ_Q is found to be governed by the inhomogeneous problem:

$$\nabla^2\varphi_Q = 0 \qquad \text{in the fluid,} \tag{5.15}$$

$$\frac{\partial\varphi_Q}{\partial n} = 0 \qquad \text{on } r = a, \tag{5.16}$$

$$\frac{\partial\varphi_Q}{\partial z} - 4\omega^2\varphi_Q = q \qquad \text{on } z = 0, \tag{5.17}$$

$$\frac{\partial\varphi_Q}{\partial y} = 0 \qquad \text{on } y = \pm 1, \tag{5.18}$$

$$\frac{\partial\varphi_Q}{\partial z} = 0 \qquad \text{on } z = -h. \tag{5.19}$$

and the radiation condition that only outgoing waves exist at infinity.

We shall apply the hybrid-element method to solve for φ_Q. For this purpose we first obtain the far-field representation by decomposing into two components: a locked wave $\varphi_Q^{(L)}$, and a free wave $\varphi_Q^{(F)}$,

$$\varphi_Q = \varphi_Q^{(L)} + \varphi_Q^{(F)}, \quad \text{large } |x|. \tag{5.20}$$

5.2.1. *Locked wave in the far field*

We define the locked wave $\varphi_Q^{(L)}$ by requiring only the inhomogeneous condition on the free surface

$$\frac{\partial\varphi_Q^{(L)}}{\partial z} - 4\omega^2\varphi_Q^{(L)} = q, \quad \text{on } z = 0, \tag{5.21}$$

and homogeneous conditions on the channel sidewalls and the bottom.

Substituting the far-field expressions (4.3) for η into (5.3), we obtain the following explicit forcing in the far fields of large $|x|$:

$$\begin{aligned} q^{\pm} &= \frac{1}{2i\omega}\sum_{m=1}^{\infty}\sum_{n=1}^{\infty}\exp((\kappa_m + \kappa_n)(\mp x + L)) \\ &\quad \times (G_{mn}\cos(m-n)\pi y - H_{mn}\cos(m+n-1)\pi y), \quad x \gtrless \pm L, \end{aligned} \tag{5.22}$$

with the coefficients

$$G_{mn} = \left(\kappa_m\kappa_n + \left(m - \tfrac{1}{2}\right)\left(n - \tfrac{1}{2}\right)\pi^2 + \tfrac{1}{2}(3\omega^4 - k^2)\right)D_m D_n, \tag{5.23}$$

$$H_{mn} = \left(\kappa_m\kappa_n - \left(m - \tfrac{1}{2}\right)\left(n - \tfrac{1}{2}\right)\pi^2 + \tfrac{1}{2}(3\omega^4 - k^2)\right)D_m D_n. \tag{5.24}$$

where the coefficients D_m are known from the first-order solution. Since κ_m, κ_n are all real and positive, the forcing function q is imaginary, as is η. Recall from (5.3) that q must be symmetric in both x and y everywhere. It follows that the locked wave potential $\varphi_Q^{(L)}$ is also symmetric in x and y, and imaginary. The far-field solution is

easily found by separation of variables,

$$\varphi_Q^{(L),\pm} = -\frac{1}{2i\omega}\sum_{m=1}^{\infty}\sum_{n=1}^{\infty}\exp((\kappa_m+\kappa_n)(\mp x+L))\left(\frac{G_{mn}\cos(m-n)\pi y}{k_{mn}^{(-)}\tan k_{mn}^{(-)}h+4\omega^2}\frac{\cos k_{mn}^{(-)}(z+h)}{\cos k_{mn}^{(-)}h}\right.$$
$$\left.+\frac{H_{mn}\cos(m+n-1)\pi y}{k_{mn}^{(+)}\tanh k_{mn}^{(+)}h-4\omega^2}\frac{\cosh k_{mn}^{(+)}(z+h)}{\cosh k_{mn}^{(+)}h}\right), \tag{5.25}$$

where

$$k_{mn}^{(-)} = ((\kappa_m+\kappa_n)^2-(m-n)^2\pi^2)^{1/2}, \tag{5.26}$$
$$k_{mn}^{(+)} = ((m+n-1)^2\pi^2-(\kappa_m+\kappa_n)^2)^{1/2}, \quad m,n\geqslant 1. \tag{5.27}$$

Note from (4.4) that

$$\kappa_m+\kappa_n < \left(m-\tfrac{1}{2}\right)\pi+\left(n-\tfrac{1}{2}\right)\pi = (m+n-1)\pi, \tag{5.28}$$

hence $k_{mn}^{(+)}$ in (5.27) is real. Taking the square of (5.26) and using (4.4), we obtain

$$\begin{aligned} k_{mn}^{(-),2} &= (\kappa_m+\kappa_n)^2-(m-n)^2\pi^2 \\ &= \left(m-\tfrac{1}{2}\right)^2\pi^2+\left(n-\tfrac{1}{2}\right)^2\pi^2-2k^2+2\kappa_m\kappa_n-m^2\pi^2+2mn\pi^2-n^2\pi^2 \\ &= 2\kappa_m\kappa_n+\frac{\pi^2}{2}-2k^2+(2mn-m-n)\pi^2. \end{aligned} \tag{5.29}$$

Since $k<\pi/2$ and $\kappa_m,\kappa_n>0$, the sum of the first three terms in the last line of (5.29) is positive. For positive integers m and n, the inequality $2mn\geqslant m+n$ is always satisfied. Hence, we find that $(k_{mn}^{(-)})^2$ is positive and $k_{mn}^{(-)}$ is real.

5.2.2. *Free wave in the far field*

In view of the symmetry of q everywhere (near and far), both $\varphi_Q^{(L)}$ and $\varphi_Q^{(F)}$ must be symmetric in both x and y. In the far field, $\varphi_Q^{(F)}$ must further behave as outgoing waves, which in turn leads to radiation damping and will render the resonance finite. Its representations can be formally written as an eigenfunction expansion,

$$\varphi_Q^{(F),\pm} = \frac{\cosh K(z+h)}{\cosh Kh}\left(\sum_{m=0}^{\overline{m}}F_{m0}^{\pm}\exp\left(\pm i\sqrt{K^2-(m\pi)^2}(x\mp L)\right)\cos m\pi y\right.$$
$$\left.+\sum_{m=\overline{m}+1}^{\infty}F_{m0}^{\pm}\exp\left(\sqrt{(m\pi)^2-K^2}(\mp x+L)\right)\cos m\pi y\right)$$
$$+\sum_{n=1}^{\infty}\frac{\cos\nu_n(z+h)}{\cos\nu_n h}\sum_{m=0}^{\infty}F_{mn}^{\pm}\exp\left(\sqrt{(m\pi)^2+\nu_n^2}(\mp x+L)\right)\cos m\pi y, \quad x\gtrless\pm L, \tag{5.30}$$

where $\overline{m}$ is the largest integer less than K/π and ν_n is a real root of

$$4\omega^2 = -\nu_n\tan\nu_n h, \quad n=1,2,\ldots. \tag{5.31}$$

The expansion coefficients $F_{mn}^{\pm}$ remain to be found.

5.2.3. *The near field and the hybrid element analysis*

In the near field, φ_Q will not be separated into free and locked waves. Since the forcing function q is symmetric in y as shown in (5.3), so is the potential φ_Q.

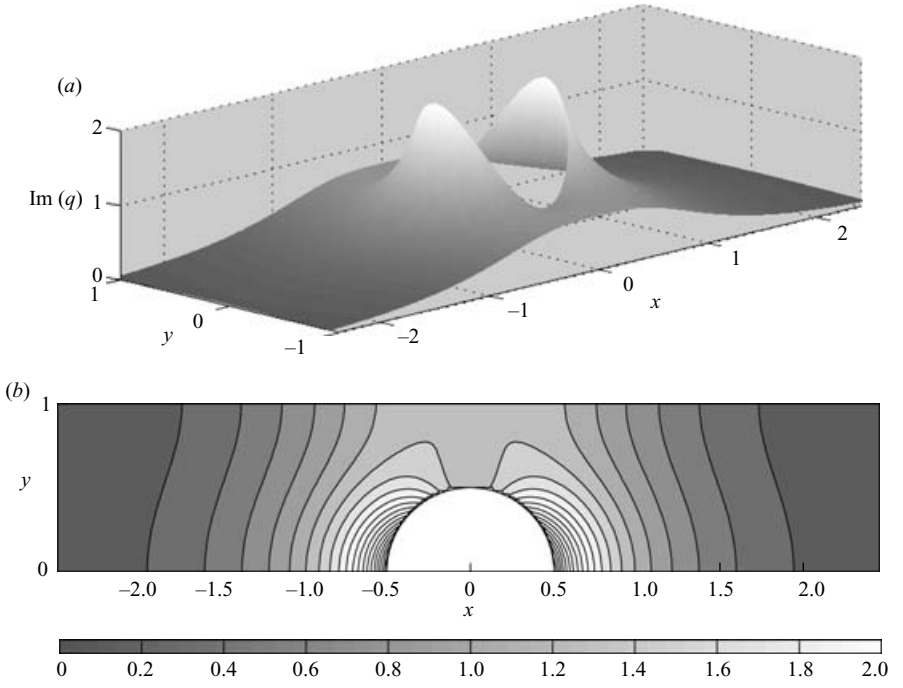

FIGURE 5. Imaginary part of the free-surface forcing, Im(q), $a = 0.5$, $\omega = 1.109$. (a) Three-dimensional plot; (b) contour plot in upper half-plane ($y > 0$). q is symmetric about $y = 0$.

This symmetry allows us to solve the boundary-value problem in the half-channel $\Omega : y \geqslant 0$. In the near field, the boundary-value problem of φ_Q can be written as

$$\nabla^2 \varphi_Q = 0 \qquad \text{in } \Omega, \tag{5.32}$$

$$\frac{\partial \varphi_Q}{\partial n} = 0 \qquad \text{on } r = a, \tag{5.33}$$

$$\frac{\partial \varphi_Q}{\partial z} - 4\omega^2 \varphi_Q = q \qquad \text{on } z = 0, \tag{5.34}$$

$$\frac{\partial \varphi_Q}{\partial z} = 0 \qquad \text{on } z = -h, \tag{5.35}$$

$$\frac{\partial \varphi_Q}{\partial y} = 0 \qquad \text{on } y = 0, \quad y = 1. \tag{5.36}$$

The near-field φ_Q will be approximated by three-dimensional finite elements with nodal unknowns. Along the borders $x = \pm L$, φ_Q of the near field and its x-derivative must match $\varphi_Q^L + \varphi_Q^F$ and its x-derivative of the far field. The combined problem for the entire channel is converted to a variational problem, as shown in Appendix A. Extremization leads to a linear matrix equation for the nodal unknowns and the expansion coefficients, and is then calculated numerically.

We first display in figure 5 some typical numerical results of the second-order forcing (5.3) due to the quadratic interaction of trapped wave. A contour plot of the complex spatial factor φ_Q on the free surface is shown in figure 6.

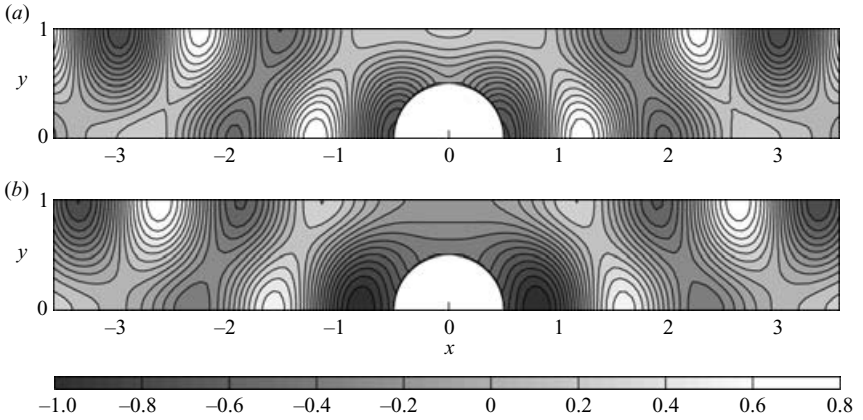

FIGURE 6. φ_Q on the free surface, $a = 0.5$, $2\omega = 2.218$, $h = 1.0$. (a) Real part; (b) imaginary part. φ_Q is symmetric about $y = 0$.

6. Evolution equation of trapped mode

At the order $O(\epsilon^2)$, the free-surface condition is inhomogeneous, as given in (3.4) and (3.8). It is easy to see that forcing on the free surface contains first and third harmonics in time,

$$\mathscr{F}_3 = \mathscr{F}_{31}\mathrm{e}^{-\mathrm{i}\omega t} + \mathscr{F}_{33}\mathrm{e}^{-3\mathrm{i}\omega t} + *, \tag{6.1}$$

Details of $\mathscr{F}_{31}$ are given in Appendix B, where it is seen that $\mathscr{F}_{31}$ decays exponentially in $|x|$ as the trapped wave. Let the third-order wave potential be expressed by

$$\Phi_3 = \varphi_{31}(x, y, z)\mathrm{e}^{-\mathrm{i}\omega t} + \varphi_{33}(x, y, z)\mathrm{e}^{-3\mathrm{i}\omega t} + *. \tag{6.2}$$

Substituting (6.2) into (3.3)–(3.5) and collecting only terms of the first harmonic, we find that φ_{31} satisfies the following condition on the free surface

$$\frac{\partial \varphi_{31}}{\partial z} - \omega^2 \varphi_{31} = \mathscr{F}_{31}, \quad \text{on} \quad z = 0. \tag{6.3}$$

At infinity, the radiation condition assures that waves are propagating outward only. All other conditions are homogeneous.

Since ω and φ_1 are the eigenfrequency and eigenfunction of the homogeneous boundary-value problem at the first order, we must examine the solvability of the inhomogeneous problem for φ_{31}. Applying Green's theorem to φ_1 and φ_{31} over the entire fluid domain Ω, we obtain

$$\iiint_{\Omega} (\varphi_1 \nabla^2 \varphi_{31} - \varphi_{31} \nabla^2 \varphi_1)\, \mathrm{d}\Omega = \iint_{\partial\Omega} \left(\varphi_1 \frac{\partial \varphi_{31}}{\partial n} - \varphi_{31} \frac{\partial \varphi_1}{\partial n} \right) \mathrm{d}S. \tag{6.4}$$

The volume integral on the left-hand side vanishes identically. After using all the boundary conditions, the surface integral on the right-hand side reduces to

$$\iint_{S_F} \varphi_1 \mathscr{F}_{31}\, \mathrm{d}S = 0 \quad \text{or} \quad \iint_{S_F} \eta \mathscr{F}_{31}\, \mathrm{d}S = 0. \tag{6.5}$$

With the lengthy details of $\mathscr{F}_{31}$ and the integration given in Appendix B, we state only the final result

$$-\mathrm{i}\frac{\mathrm{d}B}{\mathrm{d}\tau} = c_\alpha B^2 B^* + c_\gamma A B^*, \tag{6.6}$$

where

$$c_\alpha = \frac{1}{E}\sum_{i=2}^{9}\iint_{S_F}\alpha_i \mathrm{Im}(\eta)\,\mathrm{d}S; \tag{6.7}$$

$$c_\gamma = \frac{1}{E}\sum_{i=2}^{4}\iint_{S_F}\gamma_i \mathrm{Im}(\eta)\,\mathrm{d}S, \tag{6.8}$$

with

$$E = \iint_{S_F}\mathrm{Im}^2(\eta)\,\mathrm{d}S. \tag{6.9}$$

Details of the functions $\alpha_i(x, y), i = 2, 3, \ldots, 9$ and $\gamma_i(x, y), i = 2, 3, 4$ are given in Appendix B.

Equation (6.6) governs the slow evolution of the trapped-wave amplitude $B(\tau)$ and is of the Landau–Stuart form, as in the problems of edge waves on a beach and trapped modes around the Venice gates. In view of the mathematical similarity among these three cases, it is natural to anticipate that all trapped waves, whether around a stationary or mobile boundary, can be excited subharmonically.

If there is a small frequency detuning as given by (5.8), the Landau–Stuart equation (6.6) becomes

$$-\mathrm{i}\frac{\mathrm{d}B}{\mathrm{d}\tau} = c_\alpha B^2 B^* + c_\gamma \mathrm{e}^{-2\mathrm{i}\Omega\tau} B^*. \tag{6.10}$$

With the transformation

$$B = \bar{B}\mathrm{e}^{-\mathrm{i}\Omega\tau}, \tag{6.11}$$

(6.10) becomes

$$-\mathrm{i}\frac{\mathrm{d}\bar{B}}{\mathrm{d}\tau} = c_\alpha|\bar{B}|^2\bar{B} + \Omega\bar{B} + c_\gamma\bar{B}^*. \tag{6.12}$$

The mathematical properties of this Landau–Stuart equation have been studied by Rockliff (1978) for edge waves. We shall therefore only highlight the physical meaning of these coupling coefficients in the following section, to prepare the ground for examining the effects of cylinder/channel geometry on the resonance physics.

7. Physical roles of the coupling coefficients

7.1. $\mathrm{Im}(c_\alpha)$ *and radiation damping*

Multiplying B^* on both sides of (6.6) and subtracting its complex conjugate, we obtain

$$\frac{\mathrm{d}|B|^2}{\mathrm{d}\tau} = 2\mathrm{Im}(c_\gamma^* A^* B^2) - 2\mathrm{Im}(c_\alpha)|B|^4. \tag{7.1}$$

The first term on the right-hand side of (7.1) represents the energy influx to the trapped wave from the incident and scattered waves. If this term is positive, the trapped wave can be excited from an infinitesimal initial disturbance. The second term on the right-hand side of (7.1) arises from radiation of the second-order wave Φ_Q forced by quadratic interactions of the first-order trapped wave. For physical confirmation, we calculate below the period-averaged rate of work done by the radiated wave Φ_Q to the surrounding fluid. In the identity

$$\iiint_\Omega \frac{\partial\Phi_Q}{\partial t}\nabla^2\Phi_Q\,\mathrm{d}\Omega = \iiint_\Omega \nabla\cdot\left(\frac{\partial\Phi_Q}{\partial t}\nabla\Phi_Q\right)\mathrm{d}\Omega - \iiint_\Omega \nabla\frac{\partial\Phi_Q}{\partial t}\cdot\nabla\Phi_Q\,\mathrm{d}\Omega, \tag{7.2}$$

the left-hand side is zero. By the Gauss theorem and the boundary conditions, the first volume integral on the right-hand side reduces to two surface integrals

$$\overline{\iint_{S_\infty} \frac{\partial \Phi_Q}{\partial t}\frac{\partial \Phi_Q}{\partial n}\,\mathrm{d}S} + \overline{\iint_{S_F} \frac{\partial \Phi_Q}{\partial t}\frac{\partial \Phi_Q}{\partial z}\,\mathrm{d}S}, \tag{7.3}$$

where S_∞ includes two cross-sectional planes at $x \sim \pm\infty$. Physically, the negative of the first integral above is proportional to the power outflux at infinity. It follows from (7.2) and (7.3) that the power radiated to infinity is

$$\begin{aligned}
&\iint_{S_\infty}\left(-2i\omega\varphi_Q^*\frac{\partial\varphi_Q}{\partial n}+*\right)\mathrm{d}S\\
&\quad=-2i\omega\left(\iiint_\Omega \nabla\varphi_Q^*\cdot\nabla\varphi_Q\,\mathrm{d}\Omega-\iint_{S_F}\varphi_Q^*\frac{\partial\varphi_Q}{\partial z}\,\mathrm{d}S\right)+*\\
&\quad=-2i\omega\left(\iint_\Omega|\nabla\varphi_Q|^2\,\mathrm{d}\Omega-4\omega^2\iint_{S_F}|\varphi_Q|^2\,\mathrm{d}S-\iint_{S_F}q\varphi_Q^*\,\mathrm{d}S\right)+*\\
&\quad=2i\omega\iint_{S_F}q\varphi_Q^*\,\mathrm{d}S+*=-4\omega\iint_{S_F}\mathrm{Im}(q)\mathrm{Re}(\varphi_Q)\,\mathrm{d}S,
\end{aligned}\tag{7.4}$$

where the fact that q is imaginary has been used. It is shown in (B 24) of Appendix B that

$$\mathrm{Im}(c_\alpha)=-\frac{\omega}{E}\iint_{S_F}\mathrm{Im}(q)\mathrm{Re}(\varphi_Q)\mathrm{d}S. \tag{7.5}$$

Hence,

$$\iint_{S_\infty}\left(-2i\omega\varphi_Q^*\frac{\partial\varphi_Q}{\partial n}+*\right)\mathrm{d}S=4E\,\mathrm{Im}(c_\alpha). \tag{7.6}$$

Since power must be lost to infinity by radiation, it is necessary that

$$\mathrm{Im}(c_\alpha)>0, \tag{7.7}$$

which will be checked by numerical results.

7.2. $\mathrm{Re}(c_\alpha)$ *and shift of resonance frequency*

The real part of the coefficient c_α can be obtained from (6.7). The effect of $\mathrm{Re}(c_\alpha)$ is to shift the trapped mode frequency from ω to $\omega-\epsilon^2\mathrm{Re}(c_\alpha)|\bar{B}|^2$. This can be seen by rewriting (6.12) in the following form:

$$-\mathrm{i}\frac{\mathrm{d}\bar{B}}{\mathrm{d}\tau}=\mathrm{i}\mathrm{Im}(c_\alpha)|\bar{B}|^2\bar{B}+(\Omega+\mathrm{Re}(c_\alpha)|\bar{B}|^2)\bar{B}+c_\gamma\bar{B}^*. \tag{7.8}$$

When $\mathrm{Re}(c_\alpha)<0$, the natural frequency shifts to a higher value $\omega+\epsilon^2|\mathrm{Re}(c_\alpha)||\bar{B}|^2$. This is similar to a hard spring in the Duffing oscillator. If $\mathrm{Re}(c_\alpha)>0$, the shift is to a lower value $\omega-\epsilon^2|\mathrm{Re}(c_\alpha)||\bar{B}|^2$, similar to the soft spring. When $\mathrm{Re}(c_\alpha)=0$, the resonant frequency is left unchanged.

7.3. $|c_\gamma|$ *and the initial growth rate*

Starting from the rest state, nonlinearity must be unimportant at small τ. Equation (6.12) is dominated by the linear part,

$$-\mathrm{i}\frac{\mathrm{d}\bar{B}}{\mathrm{d}\tau}\approx\Omega\bar{B}+c_\gamma\bar{B}^*.$$

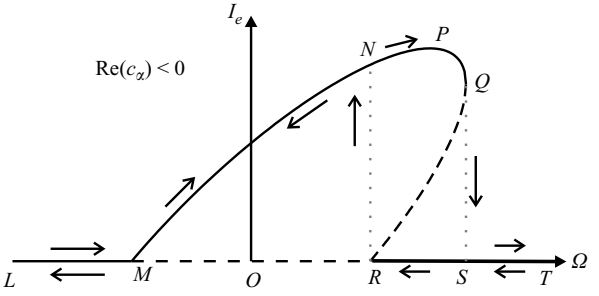

FIGURE 7. Bifurcation diagram relating the action I of equilibrium state and detuning frequency Ω when $\mathrm{Re}(c_\alpha) < 0$. —, stable branch; - - -, unstable branch. Nodes: $M = (-|c_\gamma|, 0)$, $P = (\Omega_m, I_{max})$, $Q = (|c_\alpha|/\mathrm{Im}(c_\alpha))|c_\gamma|, -(\mathrm{Re}(c_\alpha)/\mathrm{Im}(c_\alpha))/(|c_\gamma|/|c_\alpha|)$ and $R = (|c_\gamma|, 0)$.

Eliminating $\bar{B}^*$ by using the complex conjugate of the equation above, we obtain

$$\frac{\mathrm{d}^2\bar{B}}{\mathrm{d}\tau^2} - (|c_\gamma|^2 - \Omega^2)\bar{B} = 0. \tag{7.9}$$

Thus as long as detuning is weak, $|\Omega| < |c_\gamma|$, the rest state can be unstable. The growth rate is proportional to $\sqrt{|c_\gamma|^2 - \Omega^2}$ and takes the greatest value of $|c_\gamma|$ when $\Omega = 0$, i.e. perfect tuning.

7.4. *Finite equilibrium states and stability*

We shall cite the results from the nonlinear analysis of Rockliff (1978) for edge waves. Let $\bar{B}$ be expressed in polar form

$$\bar{B} = \sqrt{I}\mathrm{e}^{\mathrm{i}\theta}, \tag{7.10}$$

where $I = |\bar{B}|^2 = |B|^2$ is the action variable and θ the angle variable. The equilibrium states correspond to the solutions of (6.12) with $\mathrm{d}\bar{B}/\mathrm{d}\tau = 0$. In the bifurcation diagram of I *vs.* Ω, one such state is $I = 0$ for all Ω. There are two finite equilibrium states

$$I_e^{\pm} = \frac{-\Omega\,\mathrm{Re}(c_\alpha) \pm \sqrt{|c_\alpha|^2|c_\gamma|^2 - \mathrm{Im}^2(c_\alpha)\Omega^2}}{|c_\alpha|^2} \tag{7.11}$$

corresponding to two branches of an ellipse in the plane of I *vs.* Ω plane. The ellipse intersects the Ω-axis at two points $\Omega = \pm|c_\gamma|$. Depending on the sign of $\mathrm{Re}(c_\alpha)$, three cases can be distinguished.

Consider first $\mathrm{Re}(c_\alpha) < 0$. The ellipse is inclined to the right as shown in figure 7, and is similar to a hard spring in the Duffing oscillator. In the range of $-\infty < \Omega < -|c_\gamma|$, only the rest state $I = 0$ exists and is stable to infinitesimal disturbances. In the range $-|c_\gamma| < \Omega < |c_\gamma|$, the rest state ($I = 0$) is unstable as stated before. The finite state I_e^+ is stable. In the range of $|c_\gamma| < |\Omega| < |c_\gamma||c_\alpha|/\mathrm{Im}(c_\alpha)$, the rest state $I = 0$ is stable, as is the larger of the two finite states $I = I_e^+$. On the other hand the smaller finite state $I = I_e^-$ is unstable.

To find the maximum possible equilibrium amplitude we take the derivative of (7.11) with respect to Ω.

$$\frac{\mathrm{d}I_e^+}{\mathrm{d}\Omega} = \frac{1}{|c_\alpha|^2}\left(-\mathrm{Re}(c_\alpha) - \frac{\mathrm{Im}^2(c_\alpha)\Omega}{\sqrt{|c_\alpha|^2|c_\gamma|^2 - \mathrm{Im}^2(c_\alpha)\Omega^2}}\right) = 0. \tag{7.12}$$

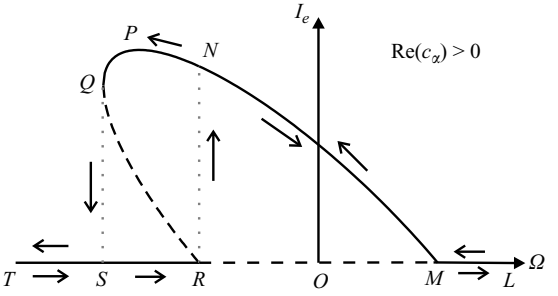

FIGURE 8. Bifurcation diagram relating the action I of equilibrium state and detuning frequency Ω when $\mathrm{Re}(c_\alpha) > 0$. —, stable branch; - - -, unstable branch. Nodes: $M = (|c_\gamma|, 0)$, $P = (\Omega_m, I_{max})$, $Q = (-(|c_\alpha|/\mathrm{Im}(c_\alpha))|c_\gamma|, (\mathrm{Re}(c_\alpha)/\mathrm{Im}(c_\alpha))(|c_\gamma|/|c_\alpha|)$ and $R = (-|c_\gamma|, 0)$.

Solving (7.12), the maximum amplitude takes place at

$$\Omega_m = -\frac{\mathrm{Re}(c_\alpha)}{\mathrm{Im}(c_\alpha)}|c_\gamma|, \tag{7.13}$$

where the conditions $\mathrm{Im}(c_\alpha) > 0$ and $\mathrm{Re}(c_\alpha) < 0$ have been used. Substituting (7.13) into (7.11), the largest action variable that can be obtained by tuning the incident wave frequency is

$$I_{max} = \frac{|c_\gamma|}{\mathrm{Im}(c_\alpha)}. \tag{7.14}$$

For comparison we note for a perfectly tuned incident wave $\Omega = 0$, the action variable is, from (7.11),

$$I_e(\Omega = 0) = \frac{|c_\gamma|}{|c_\alpha|}, \tag{7.15}$$

which is less than the maximum value except for the special case of $\mathrm{Re}(c_\alpha) = 0$.

Finally, in the range of

$$\Omega \geqslant |c_\gamma| \frac{|c_\alpha|}{\mathrm{Im}(c_\alpha)},$$

the only equilibrium state is $I = 0$ which is always stable.

For $\mathrm{Re}(c_\alpha) > 0$, the bifurcation curve leans to the left-hand side as shown in figure 8, and is similar to a soft spring in the Duffing oscillator.

In both cases discussed above, there is the jump phenomenon when the detuning frequency is varied adiabatically. This prediction has been verified in experiments for the similar problem of the Venice gates (Sammarco *et al.* 1997*a*, *b*). In the special case of $\mathrm{Re}(c_\alpha) = 0$, the ellipse is upright, as shown in figure 9; there is no jump phenomenon. We remark that, both the edge waves and the Venice gates are similar only to a hard spring in the Duffing oscillator: the bifurcation ellipse leans only to the right. In the present case of a cylinder in a channel, both hard- and soft-spring behaviours are possible, depending on the geometry, as will be shown in the next section.

In summary, the resonance phenomenon is controlled by the following key parameters. Finite resonance from rest occurs only when the frequency of the incident waves is detuned within a limited range, bounded by $\pm|c_\gamma|$. Within this range, perfect tuning produces the fastest initial growth at the rate proportional to $|c_\gamma|$. The jump phenomenon is possible only if $\mathrm{Re}(c_\alpha) \neq 0$; it is present for detuning in the positive range of $|c_\gamma| < \Omega < |c_\gamma||c_\alpha|/\mathrm{Im}(c_\alpha)$ if $\mathrm{Re}(c_\alpha) < 0$, and in the negative range

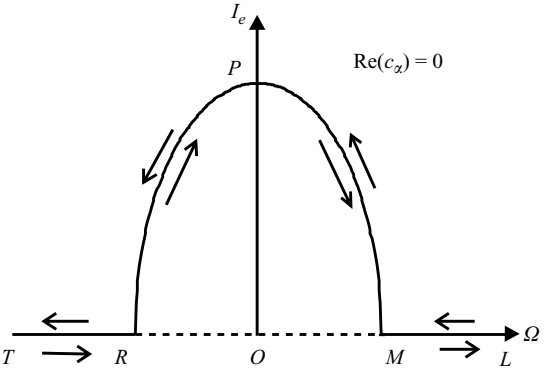

FIGURE 9. Bifurcation diagram relating the action I of equilibrium state and detuning frequency Ω when $\mathrm{Re}(c_\alpha) = 0$. —, stable branch; ---, unstable branch. Nodes: $M = (|c_\gamma|, 0)$, $P = (0, I_{max})$ is the maximum point and $R = (-|c_\gamma|, 0)$.

of $-|c_\gamma||c_\alpha|/\mathrm{Im}(c_\alpha) < \Omega < -|c_\gamma|$ if $\mathrm{Re}(c_\alpha) > 0$. In either case, the greatest equilibrium amplitude occurs when the incident wave is not perfectly tuned, and is $I_{max} = |c_\gamma|/\mathrm{Im}(c_\alpha)$.

We now examine from computed results how these key parameters are affected by geometry.

8. Effects of geometric ratios a and h

By extensive numerical computations, we can examine the effects of geometry on the resonance characteristics.

8.1. *Coefficient* c_α

The dependence of $\mathrm{Im}(c_\alpha)$ on cylinder radius a for various water depth h is plotted in figure 10. As expected, $\mathrm{Im}(c_\alpha) > 0$ always, signifying damping which renders the resonant amplitude finite. It can be seen that damping decreases as h increases; but as the cylinder radius a increases from 0 to 1, damping is the greatest for some intermediate a.

$\mathrm{Re}(c_\alpha)$, which determines the inclination of the bifurcation curve (I_e, Ω), has different signs in different parts of the (a, h)-plane, as displayed in figure 11. Within certain ranges of h, $\mathrm{Re}(c_\alpha)$ can change sign three times as a increases from 0 to 1. The bifurcation ellipse can therefore swing from left-leaning, to right-leaning and then back to left-leaning. A cylinder in a channel can therefore exhibit the behaviours of both soft and hard springs, depending on the magnitudes of a and h. This is unlike the edge wave or the Venice gates, which act like the hard spring only.

As shown in figure 10(a), when the water depth is very shallow, $h < 0.30$, there exists one peak of c_α occurring at a special a which corresponds to cutoff at $K = \pi$, see figure 3, i.e. the transition of a mode from evanescence to propagation. The appearance of a peak at cutoff is known in the linearized theory of wave–body interaction in a channel (Yeung & Sphaier 1989). For a depth in the range of $0.3 < h < 0.4445$, there can be two peaks, with the second (very mild) peak near $a = 1$. The two radii corresponding to these peaks are also associated with the same cutoff $K = \pi$, as can be seen in figure 3. For still larger depths, sharp peaks disappear, since there is no more cutoff.

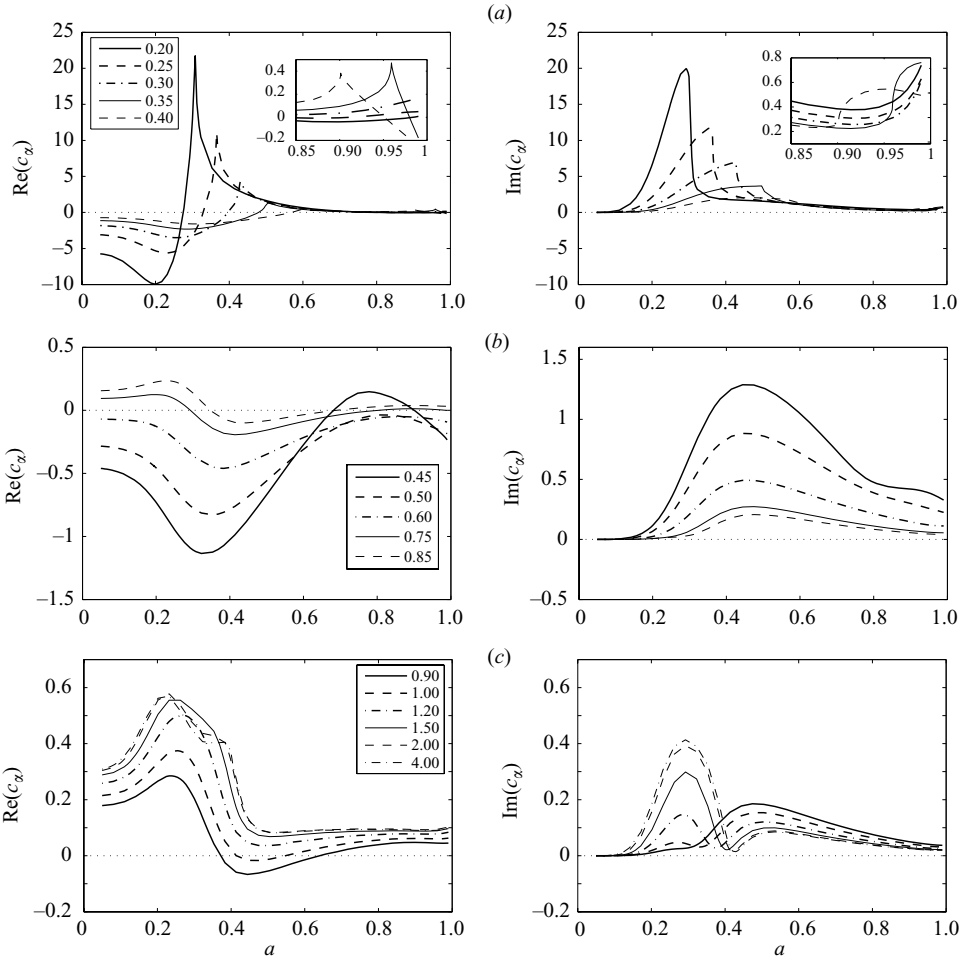

FIGURE 10. Real and imaginary parts of the coefficient $c_\alpha(a, h)$ for various water depth h. (a) Small depth: $0.20 \leqslant h \leqslant 0.40$. ($b$) Intermediate depth: $0.45 \leqslant h \leqslant 0.85$. ($c$) Large depth: $h \geqslant 0.90$.

8.2. *Coefficient* c_γ

In figure 12, we display for three ranges of depth the effects of a on $|c_\gamma|$, which is the half-range of resonant detuning frequency. Being affected also by the solution to the linear diffraction problem, c_γ shares the features of c_α. As shown in figure 12(a), when the water is shallower than 0.30, there is one sharp peak in the curves of c_γ *vs.* a. When $0.30 < h < 0.4445$, there are two peaks. Again, these peaks occur at the values of a corresponding to cutoff. When $0.45 \leqslant h \leqslant 0.85$, the curves vary smoothly with a.

8.3. *Maximum trapped-wave amplitude*

The largest trapped wave can be obtained by choosing the detuning parameter Ω to be (7.13). The maximum trapped-wave amplitude for given cylinder radius and water depth is then $|B|_{max} = \sqrt{I_{max}}$ with I_{max} given by (7.14). For various cylinder radii and water depths, the maximum trapped-wave amplitudes are plotted in figure 13.

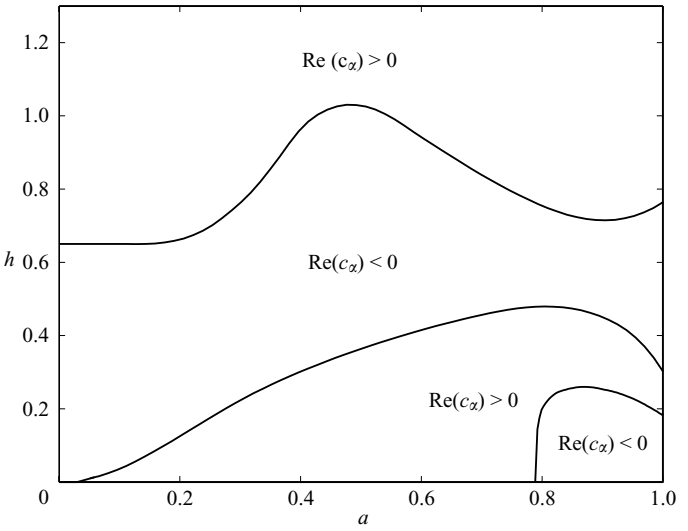

FIGURE 11. Sign of $\mathrm{Re}(c_\alpha)$ as a function of geometry.

From figure 13, the maximum trapped-wave amplitude $|B|_{max}$ becomes unboundedly large when the cylinder radius becomes very small. In theory, the trapped mode approaches a transversely standing wave with undiminishing amplitude as $x \to \pm\infty$. However, at this limit, the frequency range of resonance diminishes to zero with $|c_\gamma|$ as seen in figure 12. The trapping phenomenon itself disappears.

When $h < 0.30$, the incident wavenumber K approaches the cutoff wavenumber π once at $a = 0.3$–0.4 depending on the water depth. This explains the presence of a sudden jump of $|B|_{max}$ near $a = 0.3$–0.4 in figure 13(a). When $0.3 < h < 0.4445$, K equals the cutoff value π twice when a is between 0.50 and 0.60, and $a > 0.9$, as shown in figure 3. For very large depth, the maximum amplitude has a high peak near $a = 0.4$, which occurs when radiation damping $\mathrm{Im}(c_\alpha)$ is small, see figure 10(c).

9. Concluding remarks

As mentioned in § 1, the present geometry can be interpreted as one period in an infinite array of identical and equally spaced cylinders. By considering a large but finite number of cylinders, as Maniar & Newman (1997), finite resonance can be achieved by a linearized diffraction theory. However, the limit of an infinite number of cylinders leads to unbounded resonance, hence is a mathematical singularity. The present approach of subharmonic resonance can be regarded as a resolution of such a singularity, as nonlinearity yields finite resonance. In addition, our study provides more evidence that a trapped wave near a periodic array of bodies, whether fixed or mobile, can be resonated subharmonically in much the same way. The evolution equation is of the Landau–Stuart form; only the coupling coefficients depend on the specifics of the problem. For non-cylindrical bodies, the present hybrid-element scheme can be straightforwardly extended for computing these coefficients.

In addition, we remark first that resonance by synchronous excitation is in principle possible through nonlinearity. If there is a normally incident plane wave of the frequency ω at order $O(1)$, then quadratic interaction with itself and with the reflected wave will generate at $O(\epsilon)$ plane waves at frequency 2ω, which can resonate

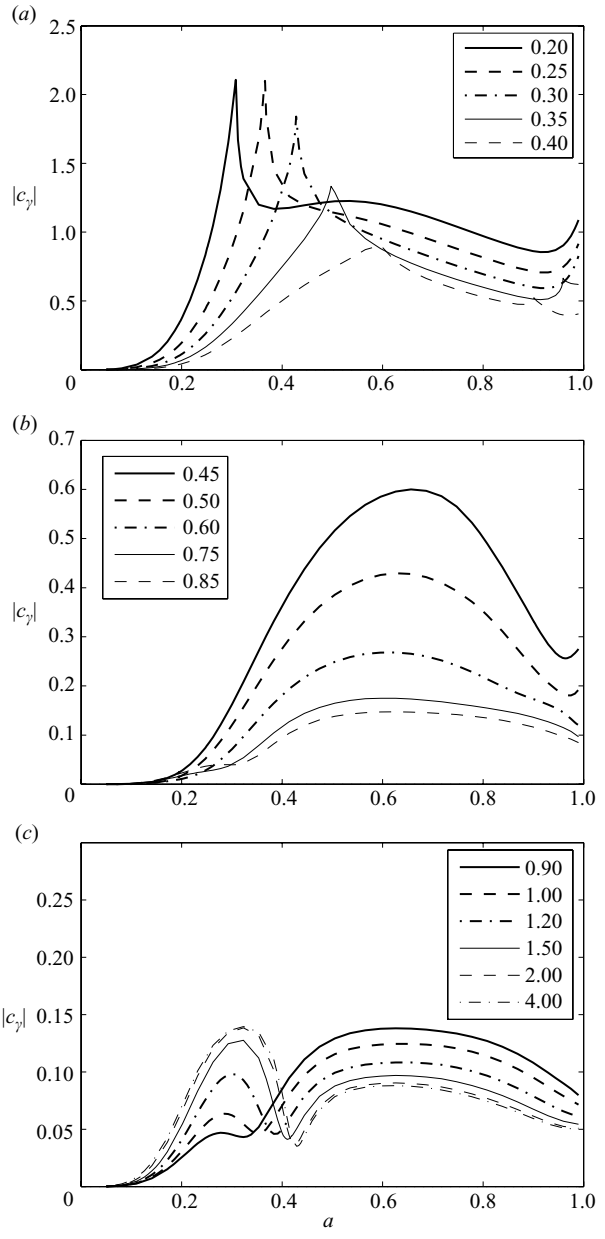

FIGURE 12. Modulus of coefficient $c_\gamma(a, h)$ for various water depth. (*a*) Small depth: $0.2 \leqslant h \leqslant 0.40$. (*b*) Intermediate depth: $0.45 \leqslant h \leqslant 0.85$. (*c*) Large depth: $h > 0.90$.

the trapped wave sub-harmonically. Secondly, for a large or infinite number of periodically spaced objects, it is known that many trapped modes can exist (see Evans & Porter 1997, 1998; Li & Mei 2003). Simultaneous nonlinear resonance of two or more modes by complex incident waves are possible. It is safe to speculate that the coupled motion is governed by a system of Landau–Stuart equations. Possibly chaotic responses of such resonances appear worthy of further investigation.

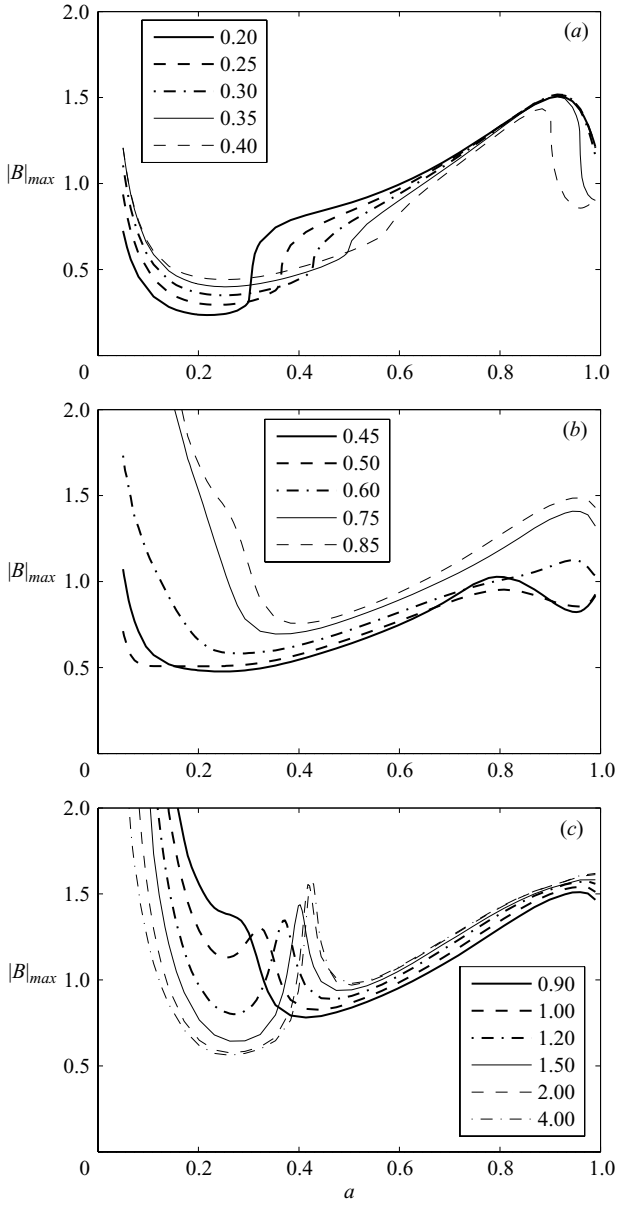

FIGURE 13. Maximum trapped wave amplitude $|B|_{max} = I_{max}^{1/2}$ for various water depths. (*a*) Small depth: $0.2 \leqslant h \leqslant 0.40$. (*b*) Intermediate depth: $0.45 \leqslant h \leqslant 0.85$. (*c*) Large depth: $h > 0.90$.

We acknowledge with gratitude the financial support the US Office of Naval Research (Grant N00014-04-1-0077), the US National Science Foundation (Grant CTS oo75713) and the US–Israel BiNational Science Foundation (Grant 2004205).

Appendix A. Variational principle for a typical scattering problem for φ

In this Appendix, we illustrate the variational principle which replaces the boundary-value problem for the second-order potential φ_Q defined in (5.15)–(5.19).

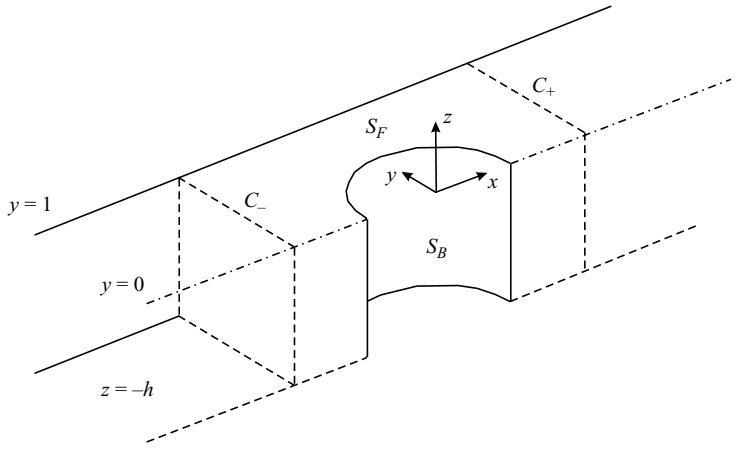

FIGURE 14. Division of fluid domains in the hybrid finite-element method.

For brevity, the subscript Q will be omitted. Modifications for other potentials are simple and will be pointed out at the end.

Let the fluid domain be divided into three regions (figure 14), the near field Ω bounded on two sides of the cylinder by two cross-sectional planes, $C_\pm : x = \pm L$, and the two far fields $\bar{\Omega}$ outside ($|x| > L$). Within Ω, φ is approximated by finite elements. In the far field $\bar{\Omega}$, the velocity potential will be distinguished by $\bar{\varphi}$ and is decomposed into the locked wave and the free wave, $\bar{\varphi} = \bar{\varphi}^L + \bar{\varphi}^F$. The locked wave $\bar{\varphi}^L$ is explicitly given by (5.25). The free wave $\bar{\varphi}^F$ is formally expressed as an eigenfunction expansion (5.30) where the coefficients $F^\pm_{mn}, m, n = 0, 1, 2, \ldots$ are to be determined. Across the interfaces $C_\pm$, the following matching conditions are required,

$$\varphi^\pm = \bar{\varphi}^\pm \big(= \bar{\varphi}^{(L),\pm} + \bar{\varphi}^{(F),\pm} \big), \tag{A 1}$$

$$\frac{\partial \varphi^\pm}{\partial n} = \frac{\partial \bar{\varphi}^\pm}{\partial n} \left(= \frac{\partial \bar{\varphi}^{(L),\pm}}{\partial n} + \frac{\partial \bar{\varphi}^{(F),\pm}}{\partial n} \right), \tag{A 2}$$

where $\varphi^\pm$ denotes $\varphi(\pm L, y, z)$.

Similar to Yue, Chen & Mei (1978), we construct the functional

$$\begin{aligned} J = {} & \frac{1}{2} \iiint_\Omega \nabla \varphi \cdot \nabla \varphi \, \mathrm{d}\Omega - \iint_{S_F} \left(\tfrac{1}{2} 4\omega^2 \varphi^2 + q\varphi \right) \mathrm{d}S \\ & - \iint_{C_\pm} \left(\varphi - \frac{\bar{\varphi}^F}{2} - \bar{\varphi}^L \right) \frac{\partial \bar{\varphi}^F}{\partial n} \, \mathrm{d}S - \iint_{C_\pm} \frac{\partial \bar{\varphi}^L}{\partial n} \varphi \, \mathrm{d}S. \end{aligned} \tag{A 3}$$

The variation of J is

$$\begin{aligned} \delta J = {} & \iiint_\Omega \nabla \varphi \cdot \nabla \delta\varphi \, \mathrm{d}\Omega - \iint_{S_F} (4\omega^2 \varphi + q) \delta\varphi \, \mathrm{d}S \\ & - \iint_{C_\pm} \left(\frac{\partial \bar{\varphi}^F}{\partial n} + \frac{\partial \bar{\varphi}^L}{\partial n} \right) \delta\varphi \, \mathrm{d}S - \iint_{C_\pm} (\varphi - \bar{\varphi}^L - \bar{\varphi}^F) \frac{\partial \delta \bar{\varphi}^F}{\partial n} \, \mathrm{d}S \\ & + \frac{1}{2} \iint_{C_\pm} \left(\delta \bar{\varphi}^F \frac{\partial \bar{\varphi}^F}{\partial n} - \bar{\varphi}^F \frac{\partial \delta \bar{\varphi}^F}{\partial n} \right) \mathrm{d}S. \end{aligned} \tag{A 4}$$

Making use of the Gauss theorem, the first integral on the right-hand side of (A 4) becomes

$$\begin{aligned}\iiint_{\Omega} \nabla\varphi\cdot\nabla\delta\varphi\,\mathrm{d}\Omega &= \iiint_{\Omega}(\nabla\cdot(\delta\varphi\,\nabla\varphi)-\delta\varphi\nabla^2\varphi)\,\mathrm{d}\Omega\\ &= \left\{\iint_{S_F}+\iint_{S_B}+\iint_{z=-h}+\iint_{y=0}+\iint_{y=1}+\iint_{C_\pm}\right\}\frac{\partial\varphi}{\partial n}\delta\varphi\,\mathrm{d}S\\ &\quad-\iiint_{\Omega}\delta\varphi\nabla^2\varphi\,\mathrm{d}\Omega. \end{aligned}\tag{A 5}$$

Substituting (A 5) into (A 4) and rearranging the terms, we obtain

$$\begin{aligned}\delta J = &-\iiint_{\Omega}\nabla^2\varphi\delta\varphi\,\mathrm{d}\Omega+\iint_{S_F}\left(\frac{\partial\varphi}{\partial z}-4\omega^2\varphi-q\right)\delta\varphi\,\mathrm{d}S\\ &+\iint_{S_B}\frac{\partial\varphi}{\partial n}\delta\varphi\,\mathrm{d}S-\iint_{z=-h}\frac{\partial\varphi}{\partial z}\delta\varphi\,\mathrm{d}S+\iint_{y=1}\frac{\partial\varphi}{\partial y}\delta\varphi\,\mathrm{d}S\\ &-\iint_{y=0}\frac{\partial\varphi}{\partial y}\delta\varphi\,\mathrm{d}S+\iint_{C_\pm}\left(\frac{\partial\varphi}{\partial n}-\frac{\partial\bar\varphi^F}{\partial n}-\frac{\partial\bar\varphi^L}{\partial n}\right)\delta\varphi\,\mathrm{d}S\\ &-\iint_{C_\pm}(\varphi-\bar\varphi^L-\bar\varphi^F)\frac{\partial\delta\bar\varphi^F}{\partial n}\,\mathrm{d}S+\frac{1}{2}\iint_{C_\pm}\left(\delta\bar\varphi^F\frac{\partial\bar\varphi^F}{\partial n}-\bar\varphi^F\frac{\partial\delta\bar\varphi^F}{\partial n}\right)\mathrm{d}S. \end{aligned}\tag{A 6}$$

In view of the governing equation and boundary conditions (5.32)–(5.36), the volume integral and the surface integrals on S_F, S_B, sea bottom $z=-h$, centreplane $y=0$, channel wall $y=1$ and interfaces $C_\pm$ of δJ vanish for arbitrary $\delta\varphi$ and $\delta\bar\varphi^F$. The last integral of (A 6) also vanishes by substituting the series expansion of $\bar\varphi^F$ and its variation from (5.30) and making use of the orthogonality of the eigenfunctions. Thus, the stationary of J is necessary for φ and $\bar\varphi_T{}^F$ to satisfy their conditions. The sufficiency of equivalence is simple and omitted.

With finite-element approximation of φ, extremization of J yields a matrix equation for the nodal unknowns and the coefficients in $\bar\varphi^F$. We omit details of the numerical implementation which are similar to Yue *et al.* (1978).

By using the appropriate far-field representations, the variational scheme can be applied to the boundary-value problems for the trapped wave φ_1 as well as the scattered wave φ_S.

Appendix B. Details of first harmonic forcing term $\mathscr{F}_{31}$ at the third order

We denote the first harmonic amplitude of the forcing term by

$$\mathscr{F}_{31}=\sum_{i=1}^{9} f_{31}^{(i)},\tag{B 1}$$

where $f_{31}^{(i)}$ is the amplitude of the first harmonic $\mathrm{e}^{-\mathrm{i}\omega t}$ of the ith term of $\mathscr{F}_3$ in (3.8).

The first term in (3.8) gives

$$-2\frac{\partial^2\Phi_1}{\partial t\,\partial\tau}=\eta\frac{\mathrm{d}B}{\mathrm{d}\tau}\mathrm{e}^{-\mathrm{i}\omega t}+*,\quad\text{hence}\quad f_{31}^{(1)}=\eta\frac{\mathrm{d}B}{\mathrm{d}\tau}.\tag{B 2}$$

The second, third and fourth terms of (3.8) contain quadratic products of Φ_1 and Φ_2, while the fifth to ninth terms contain triple products of Φ_1. Hence, the solvability

condition leads to the following Landau–Stuart equation:

$$\left[\iint_{S_F} \eta^2 \,\mathrm{d}S\right] \frac{\mathrm{d}B}{\mathrm{d}\tau} + \left[\sum_{i=2}^{9} \iint_{S_F} \alpha_i \eta \,\mathrm{d}S\right] |B|^2 B + \left[\sum_{i=2}^{4} \iint_{S_F} \gamma_i \eta \,\mathrm{d}S\right] AB^* = 0,$$

where the coefficients functions $\alpha_i(x, y)$ are defined by

$$\alpha_2 = \tfrac{1}{4}\eta\left(\frac{\partial^2 \varphi_Q}{\partial z^2} - 4\omega^2 \frac{\partial \varphi_Q}{\partial z}\right), \quad \alpha_3 = -\tfrac{1}{2}(k^2 - \omega^4)\eta\varphi_Q, \tag{B 3), (B 4}$$

$$\alpha_4 = \tfrac{1}{2}\left(\frac{\partial \varphi_Q}{\partial x}\frac{\partial \eta}{\partial x} + \frac{\partial \varphi_Q}{\partial y}\frac{\partial \eta}{\partial y} + \omega^2 \eta \frac{\partial \varphi_Q}{\partial z}\right), \tag{B 5}$$

$$\alpha_5 = \frac{3\,\mathrm{i}}{16\omega^3}(k^2 - \omega^4)\eta\left(\left(\frac{\partial \eta}{\partial x}\right)^2 + \left(\frac{\partial \eta}{\partial y}\right)^2 + \omega^4\eta^2\right), \tag{B 6}$$

$$\alpha_6 = \frac{1}{8\mathrm{i}\omega}(k^2 - \omega^4)\omega^2\eta^3, \quad \alpha_7 = 0, \tag{B 7), (B 8}$$

$$\alpha_8 = \frac{\mathrm{i}\omega}{2}\eta\left(\left(\frac{\partial \eta}{\partial x}\right)^2 + \left(\frac{\partial \eta}{\partial y}\right)^2 + k^2\eta^2\right), \tag{B 9}$$

$$\alpha_9 = \frac{3}{8\mathrm{i}\omega}\left\{\left(\frac{\partial \eta}{\partial x}\right)^2 \frac{\partial^2 \eta}{\partial x^2} + \left(\frac{\partial \eta}{\partial y}\right)^2 \frac{\partial^2 \eta}{\partial y^2} + 2\frac{\partial \eta}{\partial x}\frac{\partial \eta}{\partial y}\frac{\partial^2 \eta}{\partial x \partial y} + \omega^4\eta\left(2\left(\frac{\partial \eta}{\partial x}\right)^2 + 2\left(\frac{\partial \eta}{\partial x}\right)^2 + k^2\eta^2\right)\right\}. \tag{B 10}$$

and $\gamma_i(x, y)$ are defined by:

$$\gamma_2 = \frac{1}{8\mathrm{i}\omega}(K^2 - 16\omega^4)\eta(\eta_I + \eta_S), \quad \gamma_3 = -\frac{1}{4\mathrm{i}\omega}(k^2 - \omega^4)\eta(\eta_I + \eta_S), \tag{B 11), (B 12}$$

$$\gamma_4 = \frac{1}{4\mathrm{i}\omega}\left(\frac{\partial \eta}{\partial x}\frac{\partial(\eta_I + \eta_S)}{\partial x} + \frac{\partial \eta}{\partial y}\frac{\partial(\eta_I + \eta_S)}{\partial y} + 4\omega^4\eta(\eta_I + \eta_S)\right). \tag{B 13}$$

Since η is purely imaginary and $\eta_I, \eta_S, \varphi_Q$ are in general complex, the coefficients α_2, α_3, α_4, γ_2, γ_3, γ_4 are complex and α_5, α_6, α_7, α_8, α_9 are all real.

Denoting

$$E = -\iint_{S_F} \eta^2 \,\mathrm{d}S = \iint_{S_F} [\mathrm{Im}(\eta)]^2 \,\mathrm{d}S, \tag{B 14}$$

which is a measure of energy,

$$c_\alpha = \frac{1}{E}\sum_{i=2}^{9} \iint_{S_F} \alpha_i \,\mathrm{Im}(\eta)\,\mathrm{d}S, \tag{B 15}$$

and

$$c_\gamma = \frac{1}{E}\sum_{i=2}^{4} \iint_{S_F} \gamma_i \,\mathrm{Im}(\eta)\,\mathrm{d}S, \tag{B 16}$$

We obtain

$$-\mathrm{i}\frac{\mathrm{d}B}{\mathrm{d}\tau} = c_\alpha B^2 B^* + c_\gamma AB^*. \tag{B 17}$$

All the free-surface integrals are evaluated numerically from the hybrid-element results.

Since the coefficients $\alpha_i, i = 5, 6, \ldots, 9$ are real and η is purely imaginary, the imaginary part of the coefficient c_α is

$$\begin{aligned}\mathrm{Im}(c_\alpha) &= \frac{1}{E}\mathrm{Im}\left[\sum_{i=2}^{9}\iint_{S_F}\alpha_i\,\mathrm{Im}(\eta)\,\mathrm{d}S\right] = \frac{1}{E}\sum_{i=2}^{4}\iint_{S_F}\mathrm{Im}(\alpha_i)\mathrm{Im}(\eta)\,\mathrm{d}S \\ &= -\frac{1}{E}\mathrm{Re}\left[\sum_{i=2}^{4}\iint_{S_F}\alpha_i\,\eta\,\mathrm{d}S\right]. \qquad \text{(B 18)}\end{aligned}$$

Replacing α_2, α_3 and α_4 by (B3), (B4) and (B5), respectively, we obtain

$$\begin{aligned}\iint_{S_F}(\alpha_2+\alpha_3+\alpha_4)\,\eta\,\mathrm{d}S = \iint_{S_F}\Bigg\{&\tfrac{1}{4}\eta^2\left(\frac{\partial^2\varphi_Q}{\partial z^2} - 4\omega^2\frac{\partial\varphi_Q}{\partial z}\right) - \tfrac{1}{2}(k^2-\omega^4)\eta^2\varphi_Q \\ &+ \tfrac{1}{2}\eta\left(\frac{\partial\eta}{\partial x}\frac{\partial\varphi_Q}{\partial x} + \frac{\partial\eta}{\partial y}\frac{\partial\varphi_Q}{\partial y} + \omega^2\eta\frac{\partial\varphi_Q}{\partial z}\right)\Bigg\}\,\mathrm{d}S. \qquad \text{(B 19)}\end{aligned}$$

Making use of the Green theorem and the governing equations and boundary conditions for η and φ_T, we obtain

$$\begin{aligned}\iint_{S_F}\eta^2\frac{\partial^2\varphi}{\partial z^2}\,\mathrm{d}S &= -\iint_{S_F}\eta^2\nabla_0^2\varphi_Q\,\mathrm{d}S \\ &= \oint_{\partial S_F}\left(\varphi_T\frac{\partial\eta^2}{\partial n_0} - \eta^2\frac{\partial\varphi_Q}{\partial n_0}\right)\mathrm{d}l - \iint_{S_F}\varphi_Q\nabla_0^2\eta^2\,\mathrm{d}S \\ &= -2\iint_{S_F}\varphi_Q\left(\eta_x^2+\eta_y^2-k^2\eta^2\right)\mathrm{d}S, \qquad \text{(B 20)}\end{aligned}$$

$$\begin{aligned}\iint_{S_F}\eta\left(\frac{\partial\eta}{\partial x}\frac{\partial\varphi_Q}{\partial x} + \frac{\partial\eta}{\partial y}\frac{\partial\varphi_Q}{\partial y}\right)\mathrm{d}S &= \frac{1}{2}\iint_{S_F}\nabla_0\varphi_Q\cdot\nabla_0\eta^2\,\mathrm{d}S \\ &= \frac{1}{2}\oint_{\partial S_F}\varphi_Q\frac{\partial\eta^2}{\partial n_0}\,\mathrm{d}l - \frac{1}{2}\iint_{S_F}\varphi_Q\nabla_0^2\eta^2\,\mathrm{d}S \\ &= -\iint_{S_F}\varphi_Q\left(\eta_x^2+\eta_y^2-k^2\eta^2\right)\mathrm{d}S, \qquad \text{(B 21)}\end{aligned}$$

where ∇_0 is the gradient operator in the plane (x, y) and n_0 is the horizontal normal vector along the boundaries.

Substituting (B 20) and (B 21) into (B 19) and replacing $\partial\varphi_Q/\partial z$ by the free-surface condition (5.17), we obtain

$$\text{(B 19)} = -\mathrm{i}\omega\iint_{S_F}\frac{\varphi_Q}{2\mathrm{i}\omega}\left(2\eta_x^2+2\eta_y^2+(3\omega^4-k^2)\eta^2\right)\mathrm{d}S - \tfrac{1}{2}\omega^2\iint_{S_F}\eta^2 q\,\mathrm{d}S. \qquad \text{(B 22)}$$

Upon comparison with (5.3), we may rewrite the integral above as

$$\text{(B 19)} = -i\omega\iint_{S_F}\varphi_Q\,q\,\mathrm{d}S - \tfrac{1}{2}\omega^2\iint_{S_F}\eta^2 q\,\mathrm{d}S. \qquad \text{(B 23)}$$

Substituting this result into (B 18) and noting that η and q are both purely imaginary, we obtain

$$\mathrm{Im}(c_\alpha) = -\frac{\omega}{E}\iint_{S_F}\mathrm{Im}(q)\mathrm{Re}(\varphi_Q)\,\mathrm{d}S. \qquad \text{(B 24)}$$

REFERENCES

Callan, M., Linton, C. M. & Evans, D. V. 1991 Trapped modes in two-dimensional waveguides. *J. Fluid Mech.* **229**, 51–64.

Evans, D. V., Levitin, M. & Vassiliev, D. 1994 Existence theorems for trapped modes. *J. Fluid Mech.* **261**, 21–31.

Evans, D. V. & Linton, C. M. 1991 Trapped modes in open channels. *J. Fluid Mech.* **225**, 153–175.

Evans, D. V. & Porter, R. 1997 Trapped modes about multiple cylinders in a channel. *J. Fluid Mech.* **339**, 331–356.

Evans, D. V. & Porter, R. 1998 Trapped modes embedded in the continuous spectrum. *Q. J. Mech. Appl. Maths* **52**, 263–274.

Evans, D. V. & Porter, R. 1999 Trapping and near-trapping by arrays of cylinders in waves. *J. Engng Maths* **35**, 149–179.

Galvin, C. J. 1965 Resonant edge waves on laboratory beaches. *EOS Trans.* **46**, 112.

Guza, R. T. & Bowen, A. J. 1976 Finite amplitude Stokes edge waves. *J. Mar. Res.* **34**, 269–293.

Guza, R. T. & Davis, R. E. 1974 Excitation of edge waves by waves incident on a beach. *J. Geophys. Res.* **79**, 1285–1291.

Kagemoto, H., Murai, M., Saito, M., Molin, B. & Malenica, S. 2002 Experimental and theoretical analysis of the wave decay along a long array of vertical cylinders. *J. Fluid Mech.* **456**, 113–135.

Li, G. & Mei, C. C. 2003 Natural modes of mobile flood gates. *Appl. Ocean Res.* **25**, 115–126.

Linton, C. M. & Evans, D. V. 1990 The interaction of waves with arrays of vertical circular cylinders. *J. Fluid Mech.* **215**, 549–569.

Linton, C. M. & Evans, D. V. 1992*a* Integral equations for a class of problems concerning obstacles in waveguides. *J. Fluid Mech.* **245**, 349–365.

Linton, C. M. & Evans, D. V. 1992*b* The interaction of waves with a row of circular cylinders. *J. Fluid Mech.* **251**, 687–708.

Linton, C. M. & Evans, D. V. 1993 The radiation and scattering of surface waves by a vertical circular cylinder in a channel. *Phil. Trans. R. Soc. Lond.* A **338**, 325–357.

McIver, P. & Bennett, G. S. 1993 Scattering of water waves by axisymmetric bodies in a channel. *J. Engng Maths* **27**, 1–29.

Maniar, H. D. & Newman, J. N. 1997 Wave diffraction by a long array of cylinders. *J. Fluid Mech.* **339**, 309–330.

Mei, C. C., Sammarco, P., Chan, E. S. & Procaccini, C. 1994 Subharmonic resonance of proposed storm Venice gates for Venice lagoon. *Proc. R. Soc. Lond.* A **444**, 257–265.

Minzoni, A. A. & Whitham, G. B. 1977 On the excitation of edge wave on beaches. *J. Fluid Mech.* **79**, 273–287.

Retzler, C. H. 2001 Trapped modes: an experimental investigation. *Appl. Ocean Res.* **23**, 249–250.

Rockliff, N. 1978 Finite amplitude effects in free and forced edge waves. *Math. Proc. Camb. Phil. Soc.* **83**, 463–479.

Sammarco, P., Tran, H. H. & Mei, C. C. 1997*a* Subharmonic resonance of Venice gates in waves. Part 1. Evolution equation and uniform incident waves. *J. Fluid Mech.* **349**, 295–325.

Sammarco, P., Tran, H. H., Gottlieb, O. & Mei, C. C. 1997*b* Subharmonic resonance of Venice gates in waves. Part 2. Sinusoidally modulated incident waves. *J. Fluid Mech.* **349**, 327–359.

Utsunomiya, T. & Eatock Taylor, R. 1999 Trapped modes around a row of circular cylinders in a channel. *J. Fluid Mech.* **386**, 259–279.

Yeung, R. W. & Sphaier, S. H. 1989 Wave-interference effects on a truncated cylinder in a channel. *J. Engng Maths* **23**, 95–117.

Yue, D. K. P., Chen, H. S. & Mei, C. C. 1978 A hybrid element method for diffraction of water waves by three-dimensional bodies. *Intl J. Numer. Meth. Engng* **12**, 245–266.